Comparative study of different storage bed designs of a solid-state hydrogen tank

Mohamed Sakreddine Manai, Mikel Leturia, Carsten Pohlmann, Jorn Oubraham, Stéphane Mottelet, Michael Levy, Khashayar Saleh

MANUSCRIPT

for publication in

Journal of Energy Storage

Comparative study of different storage bed designs of a solid-state hydrogen tank

Manai Mohamed Sakreddine [a, b], Leturia Mikel [a], Pohlmann Carsten [b]

Oubraham Jorn [b], Mottelet Stéphane [a], Michael Levy [b], Saleh Khashayar [a*]

a) Sorbonne Universités, Université de Technologie de Compiègne, Integrated Transformations of Renewable Matter Laboratory (EA TIMR 4297 UTC-ESCOM), rue du Dr Schweitzer, 60200 Compiègne, France

b) Aaqius, 12 rue Vivienne, 75002 Paris, France

***Corresponding author: Khashayar Saleh**

Phone: **+33-3-44-23-52-74**

E-Mail: khashayar.saleh@utc.fr

Highlights

- Numerical simulation of hydrogenation in different metal hydride bed configurations
- Analysis of the effect of heat transfer management on system dynamics
- Predictive simulation to optimize heat transfer and hydrogenation rates

Abstract

This work discusses the influence of different metal hydride storage bed configurations. The objective was to design and optimize a solid-state hydrogen storage for a nonpolluting mobility.

A study of the absorption and desorption dynamics of a loose powder bed was performed first, followed by three different storage bed configurations: compacted Ti-Mn alloy powder, alternated Ti-Mn alloy compacts with stainless steel fins and compacted [Ti-Mn alloy / Stainless steel] powder mixture. A numerical model was developed to simulate the heat transfer and the hydrogen absorption and desorption rates.

The alternation and compact mixture configurations gave better heat transfer efficiencies, absorption and desorption rates and increased hydrogen storage densities. Indeed, an efficient heat transfer (between the tank and its surrounding fluid), a tailored porosity of the metal hydride storage bed and the addition of high thermal conductivity materials allowed the overall storage performance to be improved. Thus, the required time for loading/unloading hydrogen was reduced drastically. The alternation configuration would offer the additional advantage of a simple, inexpensive and efficient recycling procedure.

Key words: Solid-state hydrogen storage; numerical MATLAB based simulation; AB_2; heat and mass transfer; hydrogen storage bed design.

1 Introduction

The irreversible depletion of fossil fuels opens a debate between scientists, industry and civil society. This debate highlights the urgent need to search for alternative and renewable sources of energy. Not only does the depletion of fossil fuels push us to think about replacing them with renewable energy sources, but also the environmental crisis will have serious consequences on the way of life of human beings [1, 2].

It is therefore urgent to reduce the consumption of fossil energy and it is necessary to accelerate research of other non-polluting and renewable energy sources and carriers. Renewable resources such as wind and solar, converted to electricity can play an important role in the energy transition [3, 4]. Electricity storage is a solution to limit carbon emissions by enabling more use of intermittent renewable energy. Nowadays, solutions are available such as electrochemical accumulators, capacitors, chemical storage, as well as thermal storage. Among these solutions, hydrogen storage (chemical storage) offers an interesting potential [5-7]. In fact, hydrogen storage is generally realized via three different technologies: gas storage, liquid storage and “solid” storage [8, 9].

The storage of hydrogen in gaseous form is the most widely used technology today. This technology is mastered up to $700\,\mathrm{bar}$ [10]. Liquid storage requires hydrogen cooling to extremely low temperatures: $5\,\mathrm{K}\ (-268.15\,°\mathrm{C})$ [11]. In this context, solid-state hydrogen storage offers several advantages: reducing the risks related to pressurized storage, no need of ultra-cool temperature management, flexibility of use, safety, compact, efficiency, just to name a few [12]. The storage of hydrogen in a solid media (or solid-state storage) includes storing hydrogen either by absorption in a carrier material to form a hydride, or by surface adsorption [13, 14].

This study is focused on the storage of hydrogen in form of metal hydrides. The reaction between hydrogen and the metal alloy can be described as follows:

$$\mathrm{M} + \mathrm{x}\,\mathrm{H_2} \leftrightarrow \mathrm{MH_{2x}} + \mathrm{Heat} \qquad \textbf{(1)}$$

The reaction produces a metal hydride with heat release (exothermic reaction). In metal hydrides, hydrogen occupies the interstitial sites in the crystal structure of the metal. This interaction causes an expansion of the structure of the alloy. Generally, a

hydrogen loading at a pressure comparable to the operating pressure of an electrolyzer (about $10\ \mathrm{bar}$) [15, 16] and an unloading at the pressure of a fuel cell (about $2\ \mathrm{bar}$) [17, 18] are sought.

A large number of applications of metal hydride tanks has been reported in the literature. Bellosta von Colbe et al. [19] proposed a summary of metal hydrides applications for hydrogen storage and compression. For stationary applications, the weight of the tank does not represent a technological barrier. Consequently, the tank weight only depends on the hydrogen amount which is needed to be stored. For off-grid systems (stand-alone power systems), metal hydride systems can be a support for the integration of renewable energy sources (wind energy, photovoltaic energy, hydroelectric energy, etc.). Bielmann et al. [20] proposed an energy system for isolated sites and remote areas. This energy system included an AB_5 type metal hydride and a Li-ion battery. Song et al. [21] tested a 12 kg hydrogen storage tank for a mobile light tower used on construction sites. Finally, metal hydride tanks could also play a role in the development of smart-grid energy storage [22-26] and as a compressor [27-29].

Heat transfer management is a major factor in order to control the hydrogen loading and unloading times of a storage tank. Afzal et al. [30,31] carried out a study that groups together different heat transfer techniques: improvement of the thermal conductivity by inclusion of ENG in the metal hydride bed; increase of the heat transfer area by addition of fins and cooling tubes (to improve internal heat transfer); improvement of the external heat transfer by increasing the mass flow rate of the heat transfer fluid, etc. Bhogilla et al. [32] designed a cylindrical tank with a coil-shaped heat exchanger inside. This allows heat transfer from the system directly to the hydride bed without, passing through the outer wall (elimination of the external heat transfer resistance). The use of heat transfer tubes inside the tank was also studied by Ranong et al. [33] to show the effect of the number of tubes on heat transfer and thus on the time required for loading and unloading hydrogen. Mellouli et al. [34] and Dhaou et al. [35] studied the effect of a coil heat exchanger but also analyzed the effect of adding aluminum fins. This last technique allows a 50% performance increase compared to a basic tank configuration. In these studies, heat transfer enhancement techniques were studied experimentally and numerically. The

comparison of these techniques is required to choose and optimize the appropriate technique for a given storage system.

This study focuses on the modeling and comparison of different configurations of an AB_2 Ti-Mn alloy storage bed. The hydrogen absorption (desorption) reaction of the AB_2 metal hydride alloy is fast and the temperature can increase (decrease) rapidly at the beginning of the reaction. Therefore, the apparent kinetics is frequently limited by heat transfer phenomena. The objective of this work was to compare different heat transfer enhancement techniques in order to optimize the hydrogen storage tank dynamics. For this purpose, different configurations of the AB_2 Ti-Mn alloy storage bed were discussed and analyzed.

This work is based on the results published by Herbrig et al. [36]. The material chosen for the simulation of the absorption and desorption tests is a titanium-manganese alloy with the following chemical formula $Ti_{0.95}Zr_{0.05}Mn_{1.48}Fe_{0.08}Al_{0.01}$ (AB_2 type). This Ti-Mn alloy is also commercially called Hydralloy C5 [37-40]. It can reach a gravimetric hydrogen storage capacity of about $1.8\ \mathrm{wt\%}$ at room temperature [36]. The large volumetric capacity of this metal hydride is also an asset for automotive applications regarding the applicable volume constraints. A 2D axisymmetric numerical model was developed on MATLAB to study the limiting mechanism, which was either the external heat transfer (convective mechanism between the tank and the coolant fluid) or the internal heat transfer (conductive mechanism in the metal hydride bed). For this purpose, different simulations were performed:

- First, the model was validated by comparison with the experimental results published by Herbrig et al. [36];
- Second, the influence of the external heat transfer was studied, by modifying the heat transfer coefficient h (convective heat transfer between the tank walls and the coolant fluid). Hydrogen absorption and desorption simulations were performed on the reference configuration (**"Reference"**), which corresponds to a loose metal hydride powder bed;
- Third, different internal heat transfer enhancement techniques were simulated (compaction and/or addition of a high thermal conductivity material). The reference configuration (**"Reference"**) was compared to 3 metal hydride bed

configurations: **"Compact"**, **"Alternation"** and **"Compact mixture"**. The comparison was based on the absorption rate (apparent kinetics) as well as the total hydrogen storage capacity;

- Finally, the **Alternation** configuration (alternation of metal hydride compacts and stainless steel fins) was found to offer a good compromise between the total hydrogen storage capacity, the absorption rate and ease of implementation. This configuration was used to analyze the influence of the 2 main operating parameters, *i.e.*, temperature and pressure.

It should be noted that the simulation of multi-material configurations for heat transfer enhancement (Alternation and Compact mixture) represents a novelty in this work. It shows the role of a high thermal conductivity materials on the improvement of the hydrogen storage performance.

2 Model description and validation

2.1 Metal Hydride tank geometry

The tank considered in this work (**Figure 1**) corresponds to the configuration used by Herbrig et al. [36] to study a hydrogen storage system based on a graphite-metal hydride composite. The experimental results published by Herbrig et al. [36] are used to validate the 2D axisymmetric numerical model developed on MATLAB.

A cylindrical tank with an internal diameter of $40\ \mathrm{mm}$ is considered. The diameter of the internal chimney is $6\ \mathrm{mm}$. Hydrogen enters through this chimney to diffuse into the metal hydride storage bed. The tank wall is $8\ \mathrm{mm}$ thick and is made of stainless steel. The internal height of the storage bed is $130\ \mathrm{mm}$.

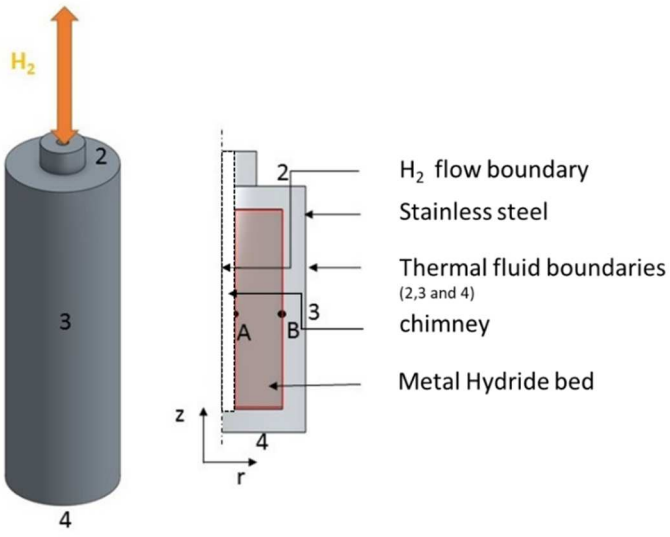

Figure 1: Simplified schematic diagram of the metal hydride tank used for the simulations (Points A and B refer to the temperature probe positions, 'core' and 'border', respectively)

2.2 Governing equations

In the present model, geometric, thermal, thermodynamic and kinetic variables are considered. This simulation takes the external solicitations, such as the variation of the hydrogen pressure and the external heating or cooling of the tank into account. Different mathematical models detailed in the literature have been developed to describe the behavior of metal hydride beds during hydrogen absorption and desorption processes [41-46]. Indeed, the mass and heat transfer simulation are essentially based on the mass and energy conservation laws, which can be expressed by partial differential equations (PDEs).

The assumptions considered in the present model are the following:

- The model is axisymmetric in a cylindrical coordinate system (r, z).
- At any location, the temperatures of the solid materials and the gas are assumed to be equal (local thermal equilibrium).
- The convective heat transfer (trough the porous medium) is negligible.
- Hydrogen behaves like an ideal gas.
- The expansion (contraction) of the metal hydride during hydrogenation (dehydrogenation) is not taken into account.

- The porosity and thermal conductivity are uniform and their variation with the absorption and desorption processes are neglected.

It is important to point out that the model considers different physical parameters for each material involved (metal hydride storage bed, tank walls, etc.). For the ease of understanding, the equations given below concern only the metal hydride storage bed.

Taking the hypothesis of local thermal equilibrium between the gas and the solid materials, a single equation of the energy balance is applicable:

$$(\rho C_p)_e \frac{\partial T}{\partial t} - \frac{1}{r}\frac{\partial}{\partial r}\left(r k_e \frac{\partial T}{\partial r}\right) - \frac{\partial}{\partial z}\left(k_e \frac{\partial T}{\partial z}\right) = -\dot{m}\,[\Delta H + T(C_{pg} - C_{ps})] \quad \textbf{(2)}$$

where T is the temperature, $(\rho C_p)_e$ is the effective thermal capacity, k_e is the effective thermal conductivity, $\dot{m}$ is the source/sink term, ΔH is the enthalpy of reaction, C_{pg} and C_{ps} are respectively the thermal capacities of the gas and the solid.

Since the hydrogenation and dehydrogenation reactions within the hydride bed are exothermic ($\Delta H < 0$) and endothermic ($\Delta H > 0$), respectively, heat is produced or consumed. Therefore, a source/sink term related to absorption/desorption $\dot{m}$ is added to the energy balance equation.

The effective heat capacity can be expressed as:

$$(\rho C_p)_e = \left[\varepsilon \rho_g C_{pg} + (1-\varepsilon)\rho_s C_{ps}\right] \quad \textbf{(3)}$$

$$(\rho_s C_{ps})_e = \left[\beta_v \rho_{steel} C_{psteel} + (1-\beta_v)\rho_{MH} C_{pMH}\right] \quad \textbf{(4)}$$

where β_v is the volumetric fraction of stainless steel in the storage bed.

The effective thermal conductivity can be calculated as:

$$k_e = \left[\varepsilon k_g + (1-\varepsilon)k_s\right] \quad \textbf{(5)}$$

$$k_s = [\beta_v k_{steel} + (1-\beta_v)k_{MH}] \quad \textbf{(6)}$$

The hydrogen gas density is calculated applying the ideal gas law:

$$\rho_g = \frac{P_g M_g}{T\,R} \quad \textbf{(7)}$$

where P_g is the hydrogen gas pressure, M_g is the molar mass of the gas and R is the universal gas constant.

The gas velocity in the bed is calculated using Darcy's law:

$$\vec{V} = -\frac{K}{\mu_g}\vec{\nabla}P \quad \textbf{(8)}$$

with:

$$\mu_g = 9{,}05 \times 10^{-6} \times \left(\frac{T}{293}\right)^{0{,}68} \quad \textbf{(9)}$$

where μ_g is the dynamic viscosity of hydrogen and K is the permeability of the metal hydride storage bed.

The continuity equation is expressed by:

$$\varepsilon \frac{\partial}{\partial t}\rho_g + \mathrm{div}\left(\rho_g \vec{V}\right) = -\dot{m} \quad \textbf{(10)}$$

After combining continuity equation **(10)**, Darcy's law **(8)** and ideal gas law **(7)**, equation **(11)** can be obtained:

$$\varepsilon \frac{M_g}{R\,T}\left(\frac{\partial P_g}{\partial t} - \frac{P_g}{T}\frac{\partial T}{\partial t}\right) = \frac{K}{\mu_g}\,\mathrm{div}\,(\rho_g \vec{\nabla}P) - \dot{m} \quad \textbf{(11)}$$

The solid mass balance is given by:

$$(1-\varepsilon)\frac{\partial \rho_s}{\partial t} = \dot{m} \quad \textbf{(12)}$$

where $\dot{m}$ corresponds to the source term of the reaction and ρ_s is the density of the metal hydride. The source term $\dot{m}$ takes a different expression for absorption and desorption.

The amount of hydrogen absorbed by the metal over time is directly related to the hydrogenation kinetics, expressed as:

$$\dot{m}_{abs} = C_a \exp\left(-\frac{E_a}{RT}\right)\ln\left(\frac{P_g}{P_{eq\_abs}}\right)(\rho_{sat} - \rho_s) \quad \textbf{(13)}$$

where C_a is the absorption kinetic constant (which depends on the material used for hydrogen storage), E_a is the activation energy for absorption, ρ_{sat} is the density of the saturated metal hydride (*i.e.*, when it has absorbed all the hydrogen that may be reversibly absorbed at a given hydrogen pressure and temperature) and P_{eq_abs} is the equilibrium pressure for absorption.

Similarly, the amount of hydrogen desorbed by the metal over time is directly related to the metal desorption kinetics, expressed by:

$$\dot{m}_{des} = C_d \exp\left(-\frac{E_d}{RT}\right)\frac{P_g - P_{eq\_des}}{P_{eq\_des}}\left(\rho_s - \rho_{emp}\right) \quad \textbf{(14)}$$

where C_d is the desorption kinetic constant, E_d is the activation energy for desorption, ρ_{emp} is the density of the metal hydride when it has desorbed all the hydrogen which can be reversibly desorbed and P_{eq_des} is the equilibrium pressure for desorption. It should be noted that the equilibrium pressure for absorption and desorption are given by equations **(21)** and **(22)** in the study of Herbrig et al. [36].

The hydrogen content is expressed as:

$$wt = \frac{\rho_s - \rho_{emp}}{\rho_s} \quad \textbf{(15)}$$

The conversion (or reacted fraction) is defined as:

$$\text{Conversion } = \frac{wt - wt_0}{wt_{max} - wt_0} \quad \textbf{(16)}$$

where wt_0 is the initial hydrogen content (before absorption) and wt_{max} is the hydrogen content of the metal hydride after complete absorption (*i.e.*, for the fully hydrogenated metal hydride).

The hydrogen is introduced axially inside the hydride bed through a porous filter. The initial and boundary conditions can be expressed as follows:

- Initial conditions:

$$\boldsymbol{T(r, z, t = 0) = T_{initial}} \quad \textbf{(17)}$$

- Boundary conditions:

$$\frac{dT(r = R, z, t)}{dr} = \frac{h}{k_e}\left(T_f - T(r = R, z, t)\right) \quad \textbf{(18)}$$

$$\frac{dT(r = 0, z, t)}{dr} = 0 \quad \textbf{(19)}$$

where h is the heat transfer coefficient and T_f is the temperature of the heating/cooling fluid surrounding the tank.

2.3 Model validation

The same parameters and simulation conditions as those defined by Herbrig et al. [36] were used to validate the mathematical model developed in the present work. A hydrogen loading simulation was reproduced and compared to the experimental results published by Herbrig et al. [36]. The cooling fluid temperature was set to $50\ °C$ and the hydrogen pressure was $40\ \mathrm{bar}$ (**Figure 2**). The key parameters of the simulation are shown in the **Table 1**.

As shown in **Figure 2**, the results of the simulation are in good agreement with those given by Herbrig et al. [36], with an acceptable deviation. The same temperature evolution, which reaches a maximum temperature (since the reaction is exothermic) to finally decrease until reaching the cooling temperature, is observed. At the end of the reaction (experimental results), there is a flexion point which is also visible in the simulation results. This point is the consequence of the end of the reaction. The simulated temperature is generally higher than the temperature observed during the hydrogenation experiment. Despite the lack of a complete description of the operating conditions of the experiment carried out by Herbrig et al. [36], the simulation results are still similar to the experimental results. Among the missing information is the external heat transfer coefficient (h). Also, in this simulation, the tank is supposed to be immersed in an isothermal bath with constant cooling/heating temperature.

In the following sections of this paper, this model will be used from a comparative perspective. It will allow the investigation of the influence of external and internal heat transfers. The objective is to improve the system performance characteristics (*i.e.*, total hydrogen storage capacity and absorption/desorption rates).

Table 1: Simulation parameters

Parameter	Value	Reference
C_{pMH}	500 J/(kg. K)	[36]
C_{psteel}	460 J/(kg. K)	[36]
E_a	500 J/mol	[38]
C_a	$6\ 10^6 1/s$	[38]
ΔH_{abs}	$-11.15\ 10^6$ J/kg	[36]
ΔH_{des}	$14.2\ 10^6$ J/kg	[36]
k_{MH}	1W/(m. K)	[36]
k_{steel}	15 W/(m. K)	[36]
M_{MH}	0.154 kg/mol	[36]
M_{H2}	0.02 kg/mol	[36]
ε	0.31 m^3/m^3	[36]
K	$8.1\ 10^{-15} m^2$	[36]
ρ_{emp}	6100 kg/m^3	[36]
ρ_{sat}	6212 kg/m^3	Calculated here for wt_{max}=1,8 wt%
ρ_{steel}	7900 kg/m^3	[36]
h	500 $W/(m^2. K)$	[36]

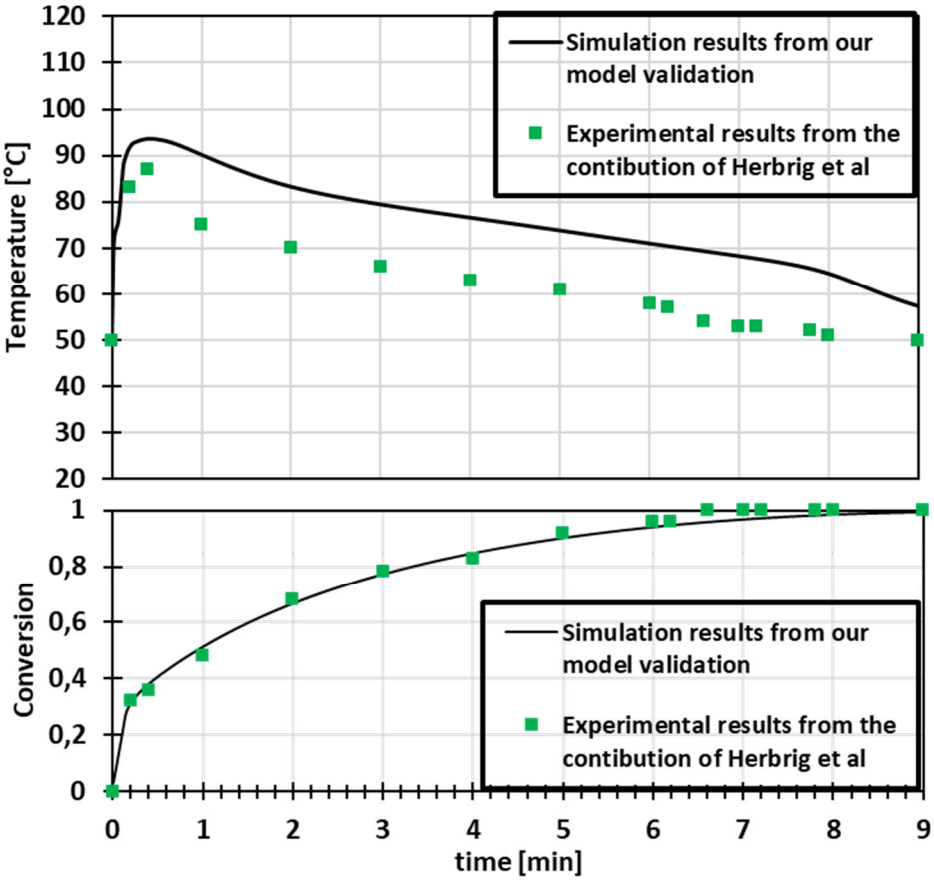

Figure 2: Simulation results for the temperature (point A in Figure 1) and conversion as a function of time during hydrogenation at 40 bar and 50°C, in comparison with experimental results of Herbrig et al. [36]

3 Description of the metal hydride bed configurations

The absorption reaction is fast, and the temperature of the reaction increases rapidly during this reaction. The apparent kinetics of the tank system is therefore limited by the reaction equilibrium. The **Reference** configuration will be used to investigate the influence of the external heat transfer (convective heat transfer between the tank walls and the coolant fluid). The other configurations (**Compact**, **Alternation** and **Compact mixture**) will be studied to show the effect of the internal heat transfer (conductive heat transfer in the metal hydride bed) on the system dynamics (absorption rate). To improve the internal heat transfer, two possible options used

separately or together will be considered: powder compaction and/or addition of a high thermal conductivity material into the hydride bed (*e.g.*, insertion of fins).

3.1 Configuration 1: "Reference"

The hydrogenation of a metal hydride powder bed is simulated. The hydrogen inlet pressure is $40\ \mathrm{bar}$ and a cooling temperature of $50\ °\mathrm{C}$ is set. The dehydrogenation simulation is performed for a heating temperature of $50\ °\mathrm{C}$ at 1 bar backpressure (the pressure and temperature values are the same as those used for the validation of the model). Metal hydride parameters for the simulation are given in **Table 1**. The hydrogen storage bed of the **Reference** configuration is shown in **Figure 3.a**.

3.2 Configuration 2: "Compact"

By compacting the powder, it is possible to reduce the porosity and, therefore, to improve the volumetric storage capacity as well as the effective thermal conductivity (equation **(5)**), *i.e.*, the internal heat transfer. The total apparent volume of metal hydride (*i.e.*, internal tank volume) is the same as in the first configuration (**Reference**). The values for porosity (0.31), permeability $(8.1\ 10^{-15}\ \mathrm{m}^2)$ and thermal conductivity of the metal hydride bed $(1.22\ \mathrm{W/(m.K)})$ are chosen according to Herbrig et al. [36]. The hydrogen storage bed of the **Compact** configuration is shown in **Figure 3.b**.

3.3 Configuration 3: "Alternation"

In the **Alternation** configuration (**Figure 3.c**), the advantage of compaction (increase of the hydrogen volumetric capacity) is kept. Furthermore, to improve internal heat transfer, a material with a high thermal conductivity (generally much higher than the metal hydride compact) is placed between each compact. The storage bed will therefore consist of an alternation of metal hydride compacts and high thermal conductivity material zones (**Figure 3.c**). Stainless steel is chosen for its low price

and high abundance. The thermal conductivity of stainless steel is 15 times greater than the thermal conductivity of the metal hydride.

The storage bed is in fact composed of 6 metal hydride compacts. Five fins are placed between the compacts. This configuration results in a mass ratio of $13\ \mathrm{wt\%}$ of stainless steel in the storage bed.

3.4 Configuration 4: "Compact mixture"

In the **Compact mixture** configuration **(Figure 3.d),** the compacts are composed of a mixture of metal hydride powder and $13\ \mathrm{wt\%}$ of stainless steel powder. The mass ratio of $13\ \mathrm{wt\%}$ of stainless steel is chosen to allow the comparison between configurations 3 and 4. The considered compacts exhibit a porosity of 0.31 (note that the compact mixture can reach the same porosity by applying a given pressure, different from the compacting pressure of the compact of configurations 2 and 3) and a permeability of $7.5\ 10^{-15}\mathrm{m}^2$ [36]. The thermal conductivity of this compacted mixture is calculated according to equations **(5)** and **(6)**.

The loading and unloading conditions are the same for all simulations: the loading (unloading) is performed under isothermal condition at $50°C$ and an inlet pressure of $40\ \mathrm{bar}$ (1 bar). The heat transfer coefficient is $h = 500\ \ \mathrm{W/(m^2.K)}$ [36].

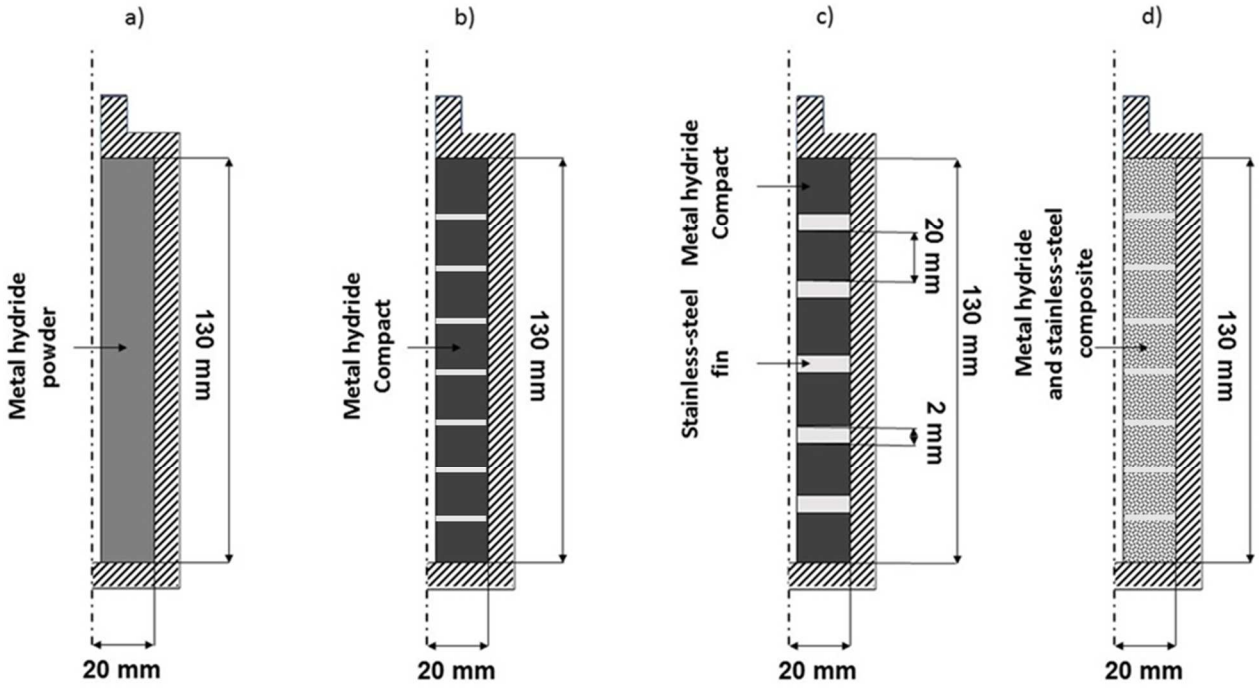

Figure 3: Schematic diagram of the different configurations of the metal hydride bed: (a) Ti-Mn alloy powder bed (1st configuration: "reference"), (b) Ti-Mn alloy compact bed (2nd configuration: "Compact"), (c) Alternation of stainless steel fins and Ti-Mn alloy compacts (3rd configuration: "Alternation") and (d) Compact of a mixture of stainless steel and metal hydride powders (4th configuration: "Compact mixture")

4 Results and discussions

One of the major controlling parameters of the solid hydrogen storage process is the heat transfer in/to the metal hydride bed. Indeed, from the thermodynamics point of view, the hydrogenation reaction can be limited without improvement of the heat transfer. To study which heat transfer resistance is limiting the apparent kinetics, various simulations on different configurations of the metal hydride bed were performed:

- First, the influence of the external heat transfer was studied, by modifying the heat transfer coefficient h (convective heat transfer between the tank walls and the coolant fluid). Hydrogen absorption and desorption simulations were performed on the **Reference** configuration;

- Second, the different internal heat transfer enhancement techniques were simulated. The **Reference** configuration was compared to the **Compact**, **Alternation** and **Compact mixture** configurations. The comparison was based on the absorption rate (apparent kinetics) as well as the total hydrogen storage capacity;
- Finally, the **Alternation** configuration was found to offer a good compromise between the total hydrogen storage capacity, the absorption rate and ease of implementation. This configuration was used to analyze the influence of the 2 main operating parameters, *i.e.*, temperature and pressure.

4.1 Influence of the external heat transfer

The influence of the heat transfer coefficient h between the storage tank and the temperature-controlled bath (surrounding the tank) is presented in this section. The range of values was chosen between 100 and $3000\ \mathrm{W/(m^2.K)}$ [36]. For comparison, the heat transfer coefficient of an air-cooled system under natural convection is between 2 and $25\ \mathrm{W/(m^2.K)}$, which can be improved up to 25 to $250\ \mathrm{W/(m^2.K)}$ under forced convection. Using oil as a cooling liquid, the effect is even more pronounced with 50 to $2000\ \mathrm{W/(m^2.K)}$ under forced convection [47]. In a nutshell, the improvement of the external heat transfer can be done by an appropriate choice of the applied cooling / heating method (natural or forced) and the used cooling fluid (air, water, oil, etc.).

Figure 4.a shows the evolution of the temperature as a function of time ($P = 40\ \mathrm{bar}$, $T_f = 50\ ^\circ\mathrm{C}$). At first, the temperature increases rapidly to reach a maximum value, followed by a slow decrease approaching the cooling temperature T_f. The temperature increases as a result of the exothermicity of the reaction. The cooling of the tank allows the temperature lowering of the metal hydride powder bed. **Figure 4.b** shows the evolution of the conversion (or reacted fraction) as a function of time. By increasing the value of the heat transfer coefficient, the reaction time for both absorption and desorption decreases. Interestingly, the external heat transfer coefficient value has a negligible influence on the magnitude of the peak

temperature. However, for large heat transfer coefficients (h), the return of the hydride bed temperature to the cooling temperature T_f is faster (**Figure 4.a**), which leads to a faster hydrogen absorption (**Figure 4.b**). These results also indicate that the internal heat transfer is a limiting factor.

The time required to reach 90% reacted fraction (conversion) during absorption and 10% reacted fraction (conversion) during desorption can be used to characterize the overall system dynamics (noted $t_{90\%\_abs}$ and $t_{90\%\_des}$ for absorption and desorption, respectively). These 2 characteristic times obtained from the simulation results are presented in **Figure 5**. The results show that there is a decrease in the loading time $t_{90\%\_abs}$ when increasing the heat transfer coefficient: for example, $668\,\mathrm{s}$ for a coefficient of $h = 100\ \mathrm{W/(m^2.K)}$ and $344\,s$ for $h = 3000\ \mathrm{W/(m^2.K)}$. For desorption (**Figure 4.c** and **Figure 4.d**), the increase of the heat transfer coefficient has a smaller effect on the unloading time $t_{90\%\_des}$.: for example, $372\,\mathrm{s}$ for a coefficient of $h = 100\ \mathrm{W/(m^2.K)}$ and $246\,\mathrm{s}$ for $h = 3000\ \mathrm{W/(m^2.K)}$.

Between $h = 100\ \mathrm{W/(m^2.K)}$ and $h = 500\ \mathrm{W/(m^2.K)}$, the increase of the heat transfer coefficient leads to a faster apparent kinetics. Above a value of $500\ \mathrm{W/(m^2.K)}$, no significant influence of the external heat transfer on the apparent kinetics is observed. Even with a 6-fold increase of this value, the time required to reach $t_{90\%\_abs}$ is not significantly reduced. It passes from $t_{90\%\_abs} = 405\,\mathrm{s}$ for a heat transfer coefficient $h = 500\ \mathrm{W/(m^2.K)}$ to $t_{90\%\_abs} = 344\,\mathrm{s}$ for a heat transfer coefficient $h = 3000\ \mathrm{W/(m^2.K)}$.

Overall, these results show that above a value of $500\ \mathrm{W/(m^2.K)}$, the internal heat transfer becomes the rate limiting step of the absorption and desorption processes. This conclusion can be explained by the poor thermal conductivity of the hydride powder. Therefore, the improvement of the internal heat transfer should be investigated by examining different configurations corresponding to different effective thermal conductivities of the hydride bed.

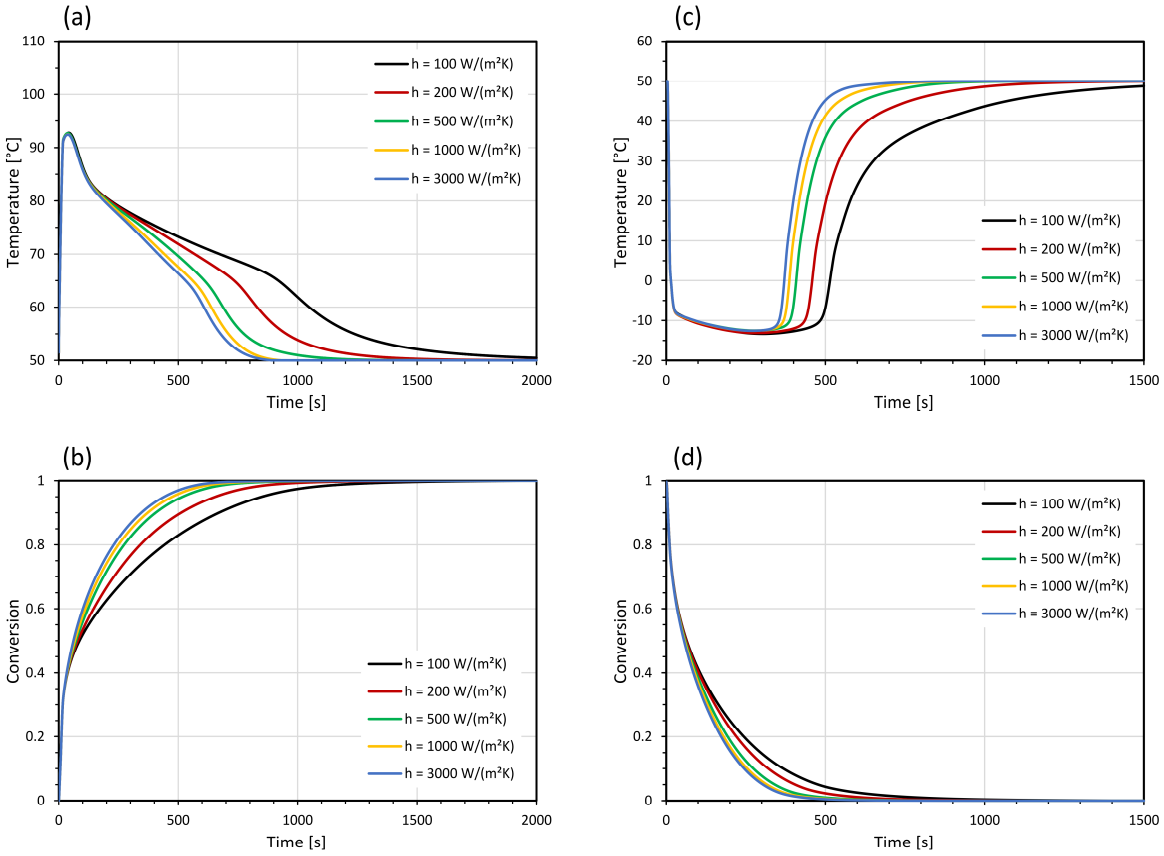

Figure 4: Simulation results of the Reference configuration, (a) Temperature at the core of the metal hydride bed (point A in Figure 1), (b) Reacted fraction during hydrogenation at 40 bar and 50 °C, (c) Temperature at the core of the metal hydride bed, (d) Reacted fraction during dehydrogenation at 1 bar and 50 °C for different heat transfer coefficient values

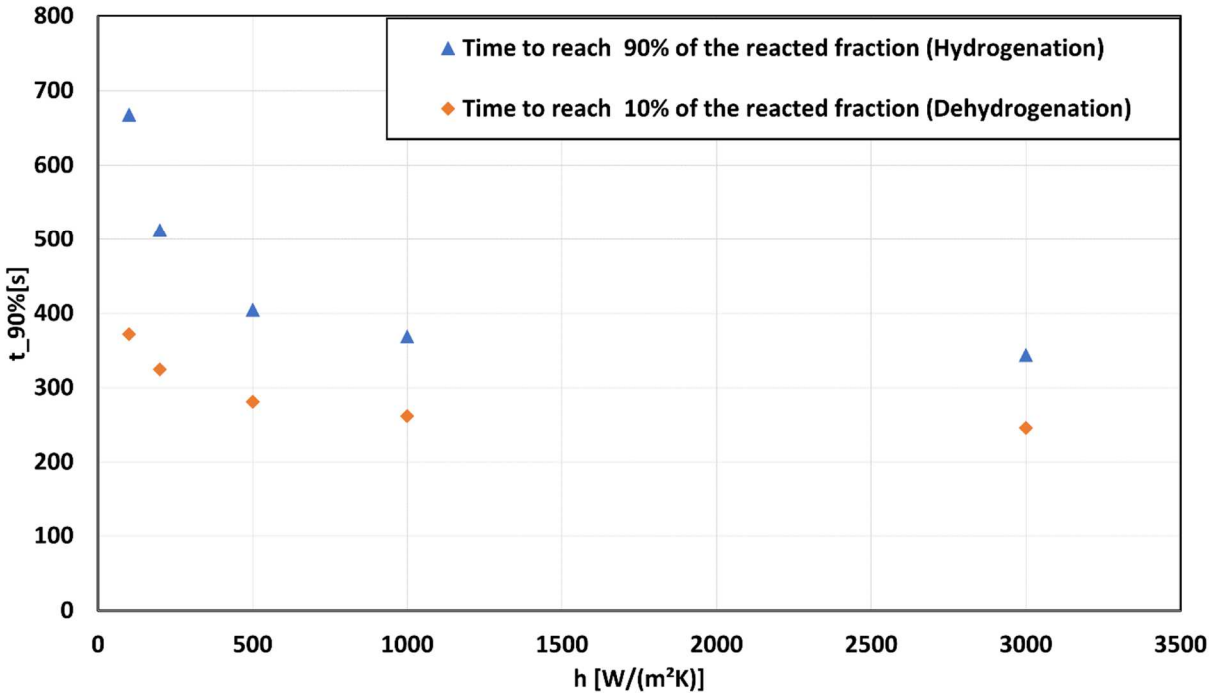

Figure 5: Hydrogenation and dehydrogenation times ($t_{90\%}$) of the Ti-Mn alloy tank system for different heat transfer coefficient values

4.2 Management of the internal heat transfer

The reduction of the porosity (compaction) of the storage bed and/or addition of a material with high thermal conductivity is suitable to tailor the internal heat transfer characteristics. For this purpose, the **Compact**, **Alternation** and **Compact mixture** configurations are studied (with $h = 500\ \mathrm{W/(m^2.K)}$, [36]). The simulation results are presented in **Figure 6** and summarized in **Table 2** ($t_{90\%\_abs}$, $t_{90\%\_des}$ and total amount of hydrogen stored).

For mobile applications, it is important that the hydrogen loading/unloading is done as quickly as possible. In this part of the work, the management of the internal heat transfer was studied for the loading step. The same conclusions would also be valid for the unloading step.

4.2.1 Configuration 2: "Compact"

Powder compaction allows a higher effective thermal conductivity and also substantially increases the amount of hydrogen that can be stored in the tank. Indeed, compacting the metal hydride powder leads to a higher apparent density of the metal hydride bed. Consequently, more metal hydride can be placed in the same tank volume, which increases the amount of hydrogen that can be stored in the tank.

The simulation results (**Figure 6**) show that by compacting the powder and reducing the porosity of the metal hydride bed, the peak temperature during hydrogen loading is less important (from $94\,℃$ for the **Reference** configuration to $88\,℃$ for the **Compact** configuration). The characteristic absorption time $t_{90\%\_abs}$ is increased, from $404\,s$ for the **Reference** configuration to $805\,s$ for the **Compact** configuration. This can be explained by the higher total metal hydride mass (**Compact** configuration), which increases the amount of hydrogen that can be stored in the tank and provokes a longer loading time.

For the same quantity of hydrogen stored, the second configuration is more efficient from the point of view of apparent kinetics. For example, for the **Reference** configuration, 4.53 g of hydrogen are stored in the tank at $t_{90\%\_abs}$ ($= 404\ \mathrm{s}$). For the **Compact** configuration, the tank only needs 44 seconds to store the same amount of hydrogen.

The effective thermal conductivity of the hydride bed is increased by 22%, from $1\ \mathrm{W/(m.K)}$ for the **Reference** configuration (loose powder) to $1.22\ \mathrm{W/(m.K)}$ for the **Compact** configuration (compacted powder) [36]. At the same time, the storage capacity increases from $5.05\ \mathrm{g}$ to $11.55\ \mathrm{g}$ (+ 130%). This necessitates to withdraw much more heat during the reaction. The increase of the effective thermal conductivity of the hydride bed alone is not sufficient to compensate for the increase of the heat released by the hydrogenation reaction. For this reason, the addition of fins in the metal hydride bed (configuration 3: **Alternation**) is considered in the following section, to further improve the internal heat transfer.

4.2.2 Configuration 3: "Alternation"

The effect of the additional fins on the absorption behavior of the metal hydride bed was tested by performing absorption simulations. As shown in **Figure 6**, the addition of fins in the "**Alternation**" configuration allows a faster heat dissipation. Indeed, it is observed that the peak temperature measured during absorption is significantly reduced. Initially, the absorption rate is higher than the heat transfer rate, and as a result, most of the energy released due to hydrogen absorption is absorbed by the hydride bed itself, which leads to a sudden rise in the bed temperature. Then, the bed temperature gradually decreases as the energy released by the reaction reaches the tank walls (external heat transfer between the tank walls and coolant fluid). The addition of fins involves the addition of heat transfer surface area into the metal hydride system. It improves the effective heat transfer characteristics by providing high thermal conductivity paths. It has a significant impact upon the performance of the reactor.

The second and the third configurations (**Compact** and **Alternation** configurations) can store approximately the same amount of hydrogen (around $11\ \mathrm{g}$).

However, the characteristic absorption time $t_{90\%\_\mathrm{abs}}$ is significantly reduced, from $805\ s$ for the **Compact** configuration to $535\ s$ for the **Alternation** configuration. Therefore, this third configuration is more efficient from the point of view of apparent kinetics. In summary, the **Alternation** configuration allows better heat transfer

characteristics, higher absorption rates (hydrogen loading rates) as well as a larger hydrogen storage capacity.

4.2.3 Configuration 4: "Compact mixture"

For the **Compact mixture** configuration, the absorption simulation (**Figure 6**) shows a temperature profile which is broadly similar to the other configurations (fast increase until a peak temperature, followed by a slow decrease approaching the cooling temperature). However, the temperature level is different. In this case, the peak temperature is similar to the one observed for the **Alternation** configuration, i.e., around $80\ °C$. The homogeneous distribution of the steel powder in the metal hydride compacts allows an important increase of the effective thermal conductivity compared to the thermal conductivity of the metal hydride compacts alone (*i.e.*, without addition of stainless steel powder). The cooling of the compact following the increase of the temperature is much faster than for any other configuration. Thus, 90% conversion is achieved in $312\ s$ ($t_{90\%\_abs}$). The addition of stainless steel powder improves the performance of the reactor, leading to better internal heat transfer and thereby reduces the bed temperature as observed in **Figure 6.a**. Also, the stainless steel powder leads to a more even temperature distribution along the metal hydride bed.

Among the three configurations studied to improve the internal heat transfer, the **Compact mixture** configuration has the strongest impact on increasing the apparent kinetics of the system. For the same tank volume, it allows a high hydrogen storage capacity with a fast absorption rate.

Table 2 summarizes the results obtained for the 4 configurations. In summary, the **Compact** configuration allows a larger hydrogen storage capacity but only a slight improvement of the internal heat transfer, compared to the **Reference** configuration. By adding fins to the compacted metal hydride powder (**Compact** configuration), the hydrogen loading rate is greatly improved and the amount of hydrogen stored is significantly increased. Of all the tested configurations, the **Compact mixture** configuration provides the fastest loading rate, with a high hydrogen storage capacity. However, it should be noted that compared to the **Alternation** configuration

(metal hydride compacts + stainless steel fins), the **Compact mixture** configuration (metal hydride + stainless steel compacted powder mixture) would be difficult to separate and recycle. Indeed, a complex and expensive procedure would be required to separate the two powders at the end of the storage tank life, resulting in a difficult recycling process. Overall, the concept of alternating compacted storage material powders with high thermal conductivity fins (**Alternation** configuration) gives the most promising results and offers a good compromise between the total hydrogen storage capacity, absorption rate and ease of implementation. This configuration will be investigated in the following section, by analyzing the influence of the 2 main operating parameters, *i.e.*, temperature and pressure.

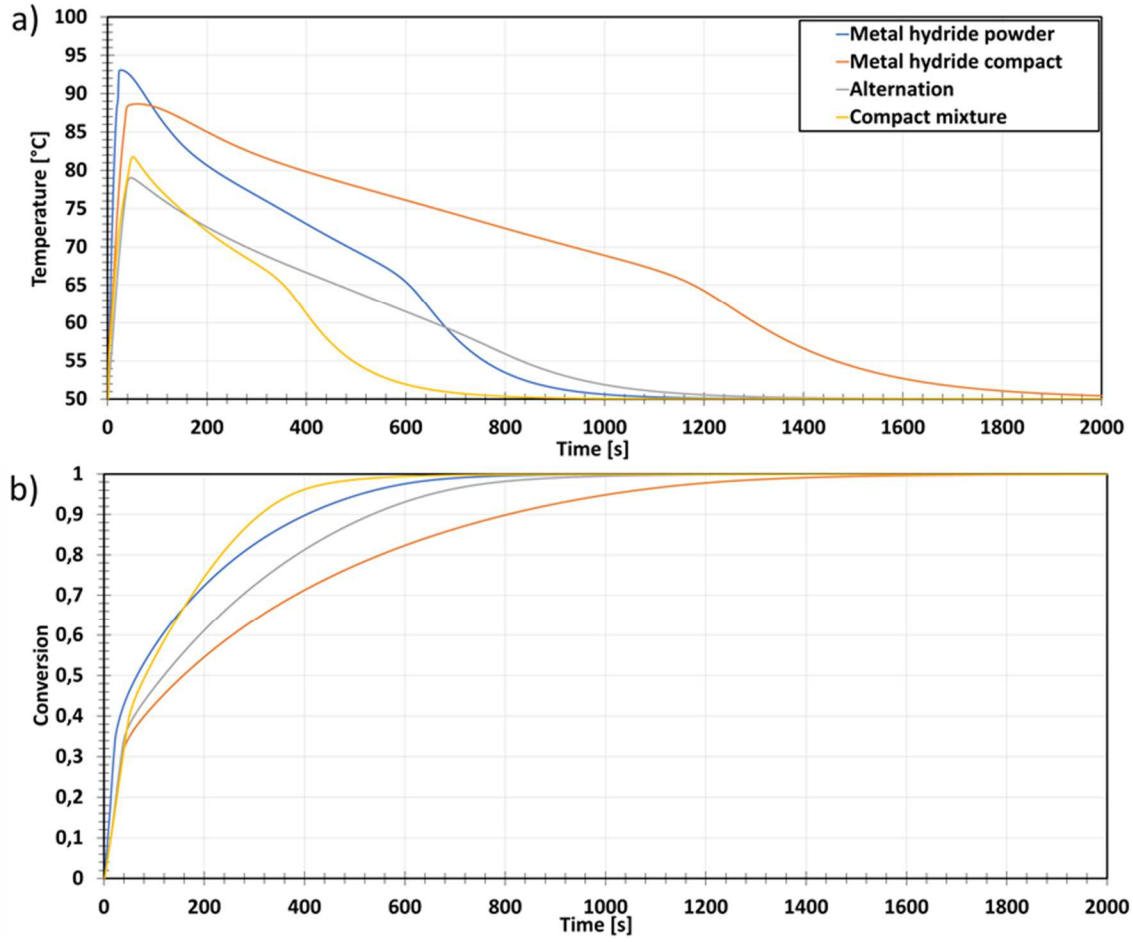

Figure 6: Simulation results for the different storage bed configurations, (a) Temperature at the core of the metal hydride bed (point A in Figure 1), (b) Reacted fraction during hydrogenation at 40 bar and 50 °C

Table 2: Characteristic times ($t_{90\%\_abs}$, $t_{90\%\_des}$) and total amount of hydrogen stored for the different tank configurations

Configuration	$t_{90\%\_abs}$ [s] hydrogenation	$t_{90\%\_des}$ [s] dehydrogenation	m_{MH} [g]	m_{bed} [g]	m_{H2_tot} [g]
1	404	280	298	298	5.05
2	805	645	682	682	11.55
3	535	440	630	725	10.67
4	312	272	630	725	10.67

4.3 Influence of the hydrogen pressure and cooling fluid temperature (Alternation configuration)

Various simulations have been performed with the **Alternation** configuration in order to investigate the influence of the hydrogen pressure and the cooling fluid temperature. The reference operating conditions used in the previous sections of this paper are $40\ \mathrm{bar}$ for the hydrogen pressure (P_g) and $50\ °\mathrm{C}$ for the cooling fluid temperature (T_f) and for the initial temperature ($T_{initial}$) of the storage bed. The corresponding results for the **Alternation** configuration were presented in **Figure 6**. Consequently, the following operating conditions have been tested:

- Hydrogen pressure: $25\ \mathrm{bar},\ 35\ \mathrm{bar}, 45\ \mathrm{bar}, 55\ \mathrm{bar},$ with a cooling fluid temperature (T_f) and an initial temperature ($T_{initial}$) of $50\ °\mathrm{C}$;
- Initial and cooling fluid temperature: $35\ °\mathrm{C}$, $45\ °\mathrm{C}$, $55\ °\mathrm{C}$, $65\ °\mathrm{C}$, with a hydrogen pressure (P_g) of $40\ \mathrm{bar}$.

The obtained results are presented in **Figure 7**. Also, it should be noted that when the pressure and temperature are changed, the amount of hydrogen absorbed at equilibrium varies (absorption isotherms are described by equations (21) and (22) in the study of Herbrig et al. [36]). The amount of hydrogen absorbed at equilibrium (*i.e.*, hydrogen storage capacity) for all the tested operating conditions are summarized in **Figure 8**.

Regarding the influence of the hydrogen pressure (P_g), the simulation results show that:

- The hydrogen storage capacity (**Figure 8**) is larger when the pressure increases (in agreement with the absorption isotherms described by equations (21) and (22) in the study of Herbrig et al. [36]). This storage capacity increase is significant between 25 and 35 bar, but is small above 35 bar;
- The hydrogen absorption rate (**Figure 7.b**) is faster at high pressures. This result is in agreement with the hydrogenation kinetics (equation **(13)**) which shows that $\dot{m}_{abs}$ increases for a larger pressure (P_g);
- The peak temperature observed at the beginning of the hydrogen absorption is also larger at high pressures (**Figure 7.a**). As the hydrogen absorption rate is faster, the heat release is also more important which leads to a higher peak temperature.

Regarding the influence of the initial and cooling fluid temperature ($T_{initial}$ and T_f), the simulation results show that:

- The hydrogen storage capacity (**Figure 8**) is larger when the temperature decreases (again in agreement with the absorption isotherms described by equations (21) and (22) in the study of Herbrig et al. [36]). This storage capacity is almost constant between 35 and 55 °C, and clearly decreases above 55 °C;
- The hydrogen absorption rate (**Figure 7.d**) is faster at low temperatures. As explained in sections 4.1 and 4.2 of this paper, the bed temperature increases rapidly at the beginning of the absorption as a result of the exothermicity of the reaction. As a consequence, the apparent hydrogenation kinetics can be limited by the reaction equilibrium and the internal and external heat transfers need to be improved to obtain faster apparent kinetics. Decreasing the cooling fluid temperature increases the temperature gradient (between the tank walls and the cooling fluid), which improves the external heat transfer and leads to faster absorption rates ;
- The peak temperature observed at the beginning of the hydrogen absorption is larger at high temperatures (**Figure 7.c**). Indeed, starting from a higher initial temperature and using a higher cooling fluid temperature leads to higher

temperatures during the hydrogenation reaction and also a larger peak temperature.

Finally, it should be noted that the reference operating conditions ($40\ \text{bar}$ and $50\ ^{\circ}\text{C}$) chosen in this work are reasonable as they allow a high hydrogen capacity (**Figure 8**).

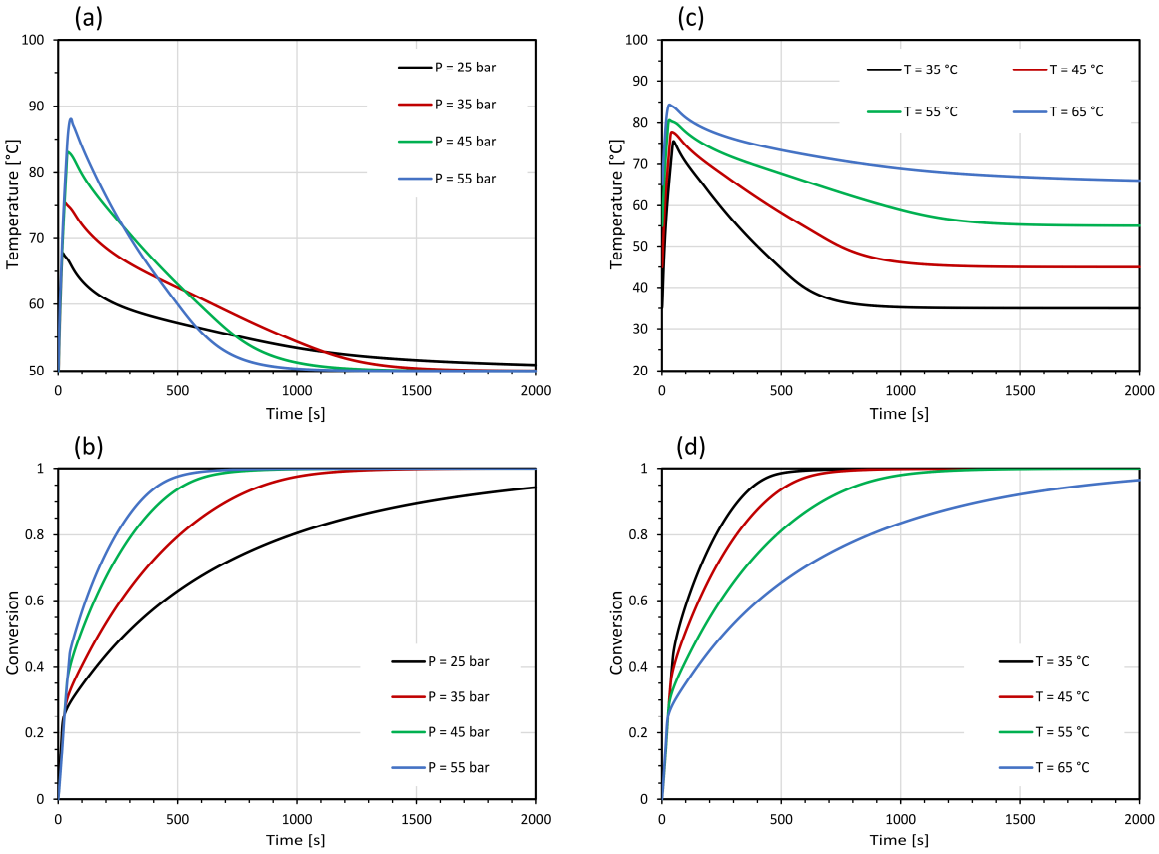

Figure 7: Simulation results for the Alternation configuration, (a) Temperature and (b) Conversion as a function of time for different hydrogen pressures, (c) Temperature and (d) Conversion as a function of time for different cooling fluid temperatures

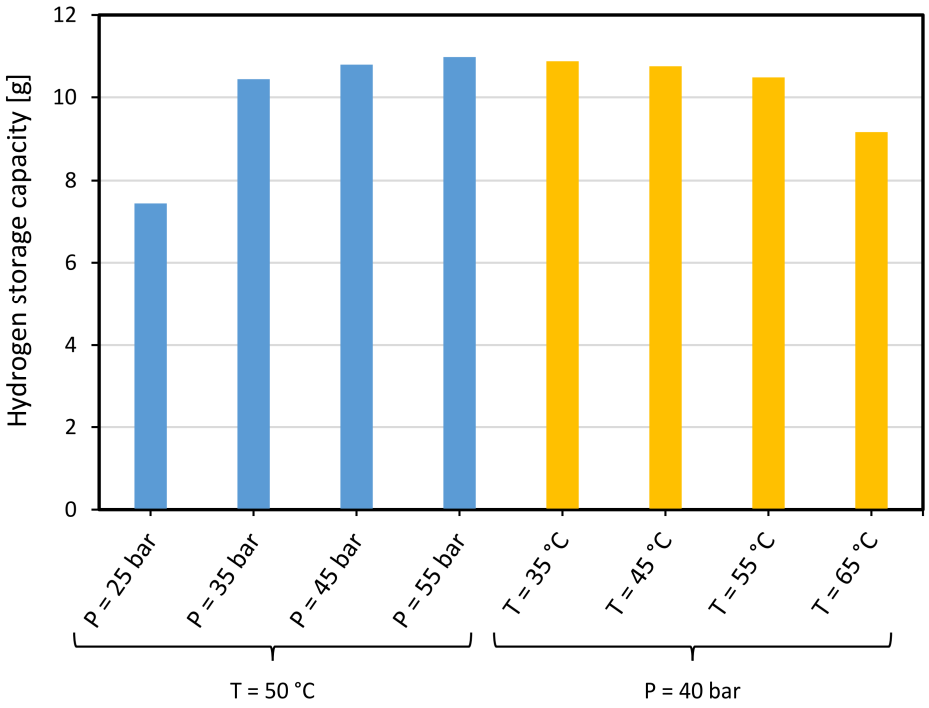

Figure 8: Hydrogen storage capacity for the Alternation configuration at various operating conditions

5 Conclusion

A MATLAB based model was developed to simulate the hydrogenation and dehydrogenation of an AB_2 metal hydride contained in a hydrogen storage tank. This 2D axisymmetric model allowed the simulation of hydrogen absorption and desorption for various tank configurations, corresponding to different heat transfer enhancement techniques (powder compaction and/or addition of high thermal conductivity materials). The challenge was to obtain fast apparent absorption and desorption rates, through better internal and external heat transfer management, while maintaining a large hydrogen volumetric capacity. The first configuration composed of a loose Ti-Mn powder (configuration 1) was considered as a **Reference** configuration. Afterwards, compacts of Ti-Mn alloy powder (configuration 2: **Compact**), an alternation of Ti-Mn alloy compacts and stainless steel fins (configuration 3: **Alternation**) and compacts of a mixture of Ti-Mn alloy and stainless steel powders (configuration 4: **Compact mixture**) were compared to evaluate their respective influence on the overall tank performance. The comparison was based on the absorption rate (apparent kinetics) as well as the total hydrogen storage capacity and ease of implementation.

External heat transfer was studied by varying the value of the external heat transfer coefficient (h) on the **Reference** configuration. For the studied system, the implementation of an external heat transfer improvement technique (such as the addition of a double wall with circulation of calorific fluid, or addition of external fins) allowed rapid cooling (heating) during absorption (desorption). However, the obtained results showed that the external heat transfer had a negligible impact on the peak temperature observed at the beginning of the hydrogen absorption or desorption process. Indeed, the low thermal conductivity of the metal hydride bed did not allow an efficient heat supply / dissipation. Thus, an analysis on the improvement of the internal heat transfer had been performed. Two techniques were studied and compared:

- The compaction of the metal hydride powder;
- The addition of a high thermal conductivity material in the form of fins or mixed powder.

The simulation results showed that the increase of the metal hydride bed thermal conductivity promoted the internal heat transfer characteristics, which improved the overall hydrogen absorption rate. The addition of a second material with high thermal conductivity was shown to be an efficient heat transfer enhancement technique. The metal hydride storage configurations (**Alternation** and **Compact mixture**) composed by both materials (metal hydride and stainless steel), showed two advantages: the improvement of internal heat transfer and the increase of the hydrogen storage capacity (for a given tank volume).

Compared to the storage bed composed by an alternation of metal hydride compacts and stainless steel fins (configuration 3: **Alternation**), the compacted powder mixture (configuration 4: **Compact mixture**) would be more difficult to separate and recycle. Therefore, the concept of alternating compacted storage material powders with high thermal conductivity fins (**Alternation** configuration) gave the most promising results and offered the best compromise between the total hydrogen storage capacity, absorption rate and ease of implementation.

Finally, various simulations were performed with the **Alternation** configuration in order to investigate the influence of the hydrogen pressure and the cooling fluid temperature. A high pressure associated to a low cooling fluid temperature gave the fastest hydrogen loading rates. From a practical point of view, the reference operating conditions ($40\ \mathrm{bar}$ and $50\ °\mathrm{C}$) chosen in this work were reasonable as they allowed a high hydrogen capacity.

References

[1] N. Nemeth, Environment and energy : problems, resolutions, solutions. Int. J. Hydrogen Energy. 15 (1990) 457–62.

[2] P. Selvam, Energy and environment-An all time search, Int. J. Hydrogen Energy. 16 (1991) 35–45.

[3] M. Paskevicius, D.A. Sheppard, K. Williamson, C.E. Buckley, Metal hydride thermal heat storage prototype for concentrating solar thermal power. Energy. 88 (2015) 469–77.

[4] G. Luderer, R.C. Pietzcker, S. Carrara, H.S. de Boer, S. Fujimori, N. Johnson, S. Mima, D. Arent, Assessment of wind and solar power in global low-carbon energy scenarios: An introduction. Energy Econ. 64 (2017) 542–51.

[5] T.A. Semelsberger, K.P. Brooks, Chemical hydrogen storage material property guidelines for automotive applications, J. Power Sources. 279 (2015) 593–609.

[6] C.L. Aardahl, S.D. Rassat, Overview of systems considerations for on-board chemical hydrogen storage, Int. J. Hydrogen Energy. 34 (2009) 6676–83.

[7] A.V. Safronov, S.S. Jalisatgi, H.B. Lee, M.F. Hawthorne, Chemical hydrogen storage using polynuclear borane anion salts, Int. J. Hydrogen Energy. 36 (2011) 234–9.

[8] A. Zuttel, A. Borgshulte, L. Schlapbach, Hydrogen as a future Energy carrier. Wiley-VCH. (2008).

[9] M. Wietschel, M. Ball, The future of hydrogen – opportunities and challenges. Int, J. Hydrogen Energy. 34 (2009) 615–27.

[10] J. Zheng, X. Liu, P. Xu, P. Liu, Y. Zhao, J. Yang, Development of high pressure gaseous hydrogen storage technologies, Int. J. Hydrogen Energy. 37 (2012) 1048–57.

[11] G. Valenti, Hydrogen liquefaction and liquid hydrogen storage, Compendium Hydrogen Energy. 23 (2016) 28-51.

[12] R. Bhattacharyya, S. Mohan, Solid state storage of hydrogen and its isotopes: An engineering overview, Renew. Sustain. Energy Rev. 41 (2015) 872–83.

[13] B. Sakintuna, F. Lamari-Darkrim, M. Hirscher, Metal hydride materials for solid hydrogen storage: A review, Int. J. Hydrogen Energy. 32 (2007) 1121–40.

[14] F.E. Lynch, Metal hydride practical applications, J. Less Common Mater. 172 (1991) 943–58.

[15] K. Sapru, S. Ramachandran, An Integrated PV – Electrolysis Metal Hydride Hydrogen Generation and Storage System, Energy Convers. (2000).

[16] V. Pérez-Herranz, M. Pérez-Page, R. Beneito, Monitoring and control of a hydrogen production and storage system consisting of water electrolysis and metal hydrides, Int. J. Hydrogen Energy. 35 (2010) 912–19.

[17] M.V. Lototskyy, I. Tolj, L. Pickering, C. Sita, F. Barbir, V. Yartys, The use of metal hydrides in fuel cell applications, Prog. Nat. Sci. Mater. Int. 27 (2017) 3–20.

[18] Z. Liu, Y. Li, Q. Bu, C.J. Guzy, Q. Li, W. Chen, C. Wang, Novel fuel cell stack with coupled metal hydride containers, J. Power Sources. 328 (2016) 329–35.

[19] J. Bellosta von Colbe, J.-R. Ares, J. Barale, M. Baricco, et al., Application of hydrides in hydrogen storage and compression: Achievements, outlook and perspectives, Int. J. Hydrogen Energy. 44 (2019) 7780–808

[20] M. Bielmann, U.F. Vogt, M. Zimmermann, A. Zuttel, Seasonal energy storage system based on hydrogen for self sufficient living, J Power Sources. 196 (2011) 4054–60.

[21] C. Song, L.E. Klebanoff, T.A. Johnson, B.S. Chao, A.F. Socha, J.M. Oros, et al., Using metal hydride H2 storage in mobile fuel cell equipment: design and predicted performance of a metal hydride fuel cell mobile light, Int. J. Hydrogen. Energy. 39 (2014) 14896–911.

[22] L. Valverde, F. Rosa, C. Bordons, J. Guerra, Energy management strategies in hydrogen smart-grids: a laboratory experience, Int. J. Hydrogen. Energy. 41 (2016) 13715–25.

[23] W. Liu, C.J. Webb, E.M. Gray, Review of hydrogen storage in AB3 alloys targeting stationary fuel cell applications, Int. J. Hydrogen. Energy. 41 (2016) 3485–507.

[24] T. Lohner, A. D'Aveni, Z. Dehouche, P. Johnson, Integration of large-scale hydrogen storages in a low-carbon electricity generation system, Int. J. Hydrogen Energy. 38 (2013) 14638–53.

[25] A.T. Thattai, B.J. Wittebrood,T Woudstra, J.J.C. Geerlings, P.V. Aravind, Thermodynamic system studies for a natural gas combined cycle (NGCC) plant with CO_2 capture and hydrogen storage with metal hydrides. Energy Procedia. 63 (2014) 1996–2007.

[26] G.L. Soloveichik, Regenerative fuel cells for energy storage, Proc. IEEE. 102 (2014) 964–75.

[27] T. Yoshida, K. Kojima, Toyota MIRAI fuel cell vehicle and progress toward a future hydrogen society. Electrochem. Soc. Interfac. 24 (2015) 45–9.

[28] S. Metz, Linde pioneers hydrogen compression techniques for fuel cell electric vehicles. Fuel Cells Bull. 2014 (2014) 12–5.

[29] X. Wang, R. Chen, Y. Zhang, C. Chen, Q. Wang, Hydrogen storage alloys for high-pressure suprapure hydrogen compressor, J. Alloy Comp . 420 (2006) 322–5.

[30] M. Afzal, R. Mane, P. Sharma, Heat transfer techniques in metal hydride hydrogen storage: A review, Int. J. Hydrogen Energy. 42 (2017) 30661–82.

[31] M. Afzal, P. Sharma, Design of a large-scale metal hydride based hydrogen storage reactor: Simulation and heat transfer optimization, Int. J. Hydrogen Energy. (2018) 1–17.

[32] S.S. Bhogilla, Design of a AB2-metal hydride cylindrical tank for renewable energy storage, J. Energy Storage. 14 (2017) 203–10.

[33] C.N. Ranong, M. Höhne, J. Franzen, J. Hapke, G. Fieg, M. Dornheim, N. Eigen, J.M. Bellosta von Colbe, O. Metz, Concept, design and manufacture of a prototype hydrogen storage tank based on sodium alanate, Chem. Eng. Technol. 32 (2009) 1154–63.

[34] S. Mellouli, F. Askri, H. Dhaou, A. Jemni, S. Ben Nasrallah, Numerical study of heat exchanger effects on charge/discharge times of metal-hydrogen storage vessel. Int. J. Hydrogen Energy. 34 (2009) 3005–17.

[35] H. Dhaou, A. Souahlia, S. Mellouli, F. Askri, A. Jemni, S. Ben Nasrallah, Experimental study of a metal hydride vessel based on a finned spiral heat exchanger, Int. J. Hydrogen Energy. 35 (2010) 1674–80.

[36] K. Herbrig, L. Röntzsch, C. Pohlmann, T. Weißgärber, B. Kieback, Hydrogen storage systems based on hydride-graphite composites: Computer simulation and experimental validation, Int. J. Hydrogen Energy. 38 (2013) 7026–36.

[37] M. Dietrich, C. Pohlmann, I. Burger, M. Linder, L. Rontzch, Long-term cycle stability of metal hydride-graphite composites, Int. J. Hydrogen Energy 46 (2015) 16375-382.

[38] I. Burger, M. Dietrich, C. Pohlmann, L. Rontzch, M. Linder, Standardized hydrogen storage module with high utilization factor based on metal hydride-graphite composites, J. Power sources. 342 (2017) 970-9.

[39] K. Herbrig, C. Pohlmann, L. Gondek, H. Figiel, N. Kardjilow et al., Investigations of the structural stability of metal hydride composites by in-situ neutron imaging, J. power sources, 293 (2015) 109-18.

[40] K. Manickmanm, D.M. Grant, G.S. Walker, Optimization of AB2 type alloy composition with superior hydrogen storage properties for stationary applications, Int. J. Hydrogen Energy. 40 (2015) 16288-296.

[41] V.M. Skripnyuk, M. Ron, Evaluation of kinetics by utilizing the normalized pressure dependence method for the alloy Ti0.95Zr0.05Mn1.48V0.43Fe0.08Al0.01, J. of Alloys and Coumpounds. 295 (1999) 385-90.

[42] A. Jemni, S. Nasrallah, J. Lamloumi, Experimental and theoretical study of a metal-hydrogen reactor, Int. J. Hydrogen Energy. 24 (1999) 631–44.

[43] G. Gwak, S. Yun, H. Ju, Multi-dimensional modeling and large-scale simulation of hydrogen absorption/desorption phenomena in metal hydride vessels (MHVs), Fusion Eng. Des. 130 (2018) 107–13.

[44] F. Askri, M. Ben Salah, A. Jemni, S. Ben Nasrallah, Optimization of hydrogen storage in metal-hydride tanks, Int. J. Hydrogen Energy. 34 (2009) 897–905.

[45] N.B. Selvaraj, D. Chapelle, D. Perreux, H. Figiel, Modelling the evolution of temperature inside LaNi4.78Sn0.22 storage tank during refueling, Mater. Des.

30 (2009) 954–7.

[46] M. Valizadeh, M.A. Delavar, M. Farhadi, Numerical simulation of heat and mass transfer during hydrogen desorption in metal hydride storage tank by Lattice Boltzmann method, Int. J. Hydrogen Energy. 41 (2015) 1–12.

[47] P. Stephan, S. Kabelac, M. Kind, H. Martin, D. Mewes, K. Schaber, VDI Heat Atlas, 2nd ed. Germany : VDI e.V. 15 (2010).

Nomenclature

C_a: absorption reaction rate coefficient, $1/\mathrm{s}$

C_d: desorption reaction rate coefficient, $1/\mathrm{s}$

C_p: specific heat capacity at constant pressure, $\mathrm{J}/(\mathrm{kg}.\mathrm{K})$

E_a: activation energy, J/mol

h: heat transfer coefficient, $\mathrm{W}/(\mathrm{m}^2.\mathrm{K})$

K: permeability, m^2

k: thermal conductivity, $\mathrm{W}/(\mathrm{m}.\mathrm{K})$

M: molar mass, g/mol

$\dot{m}$: reaction rate, $\mathrm{kg}/(\mathrm{s}.\mathrm{m}^3)$

P_g: hydrogen pressure, bar

P_{atm}: standard pressure, 1.01325 bar

R: universal gas constant, 8.3145 $\mathrm{J}/(\mathrm{mol}.\mathrm{K})$

T: temperature, K

T_f: temperature of the cooling/heating fluid, K

t: time, s

$t_{90\%\_abs}$: time to reach 90% of reacted fraction, s

$t_{90\%\_des}$: time to reach 10% of reacted fraction, s

V: gas velocity, m/s

Greek

ΔH: enthalpy of reaction per mole, J/kg

ε: porosity, –

ρ: mass density, kg/m^3

μ_g*:* dynamic viscosity, $\mathrm{Pa}\,.\,\mathrm{s}$

Subscripts

abs: absorption

axi: axial

des: desorption

eff: effective (bulk)

eq: equilibrium

H: hydrogen

i: index